ACS APPLIED MATERIALS & INTERFACES

Research Article

www.acsami.org

Discriminative Power of Chemically Sensitive Silicon Nanowire Field Effect Transistors to Volatile Organic Compounds

Rotem Ermanok, Ossama Assad, Keren Zigelboim, Bin Wang, and Hossam Haick*

The Department of Chemical Engineering and Russell Berrie Nanotechnology Institute, Technion-Israel Institute of Technology, Haifa 3200003, Israel

ABSTRACT: We report on the sensing of different polar and nonpolar volatile organic compounds (VOCs) in an atmosphere with background humidity (relative humidity: 40%), using molecularly modified silicon nanowire field effect transistors (SiNW FETs). In this endeavor, a systematic comparative analysis is performed with: (i) SiNW FETs that were functionalized with a series of molecules having different electron-withdrawing and electron-donating end groups; and (ii) SiNW FETs that are functionalized with a series of molecules having similar functional groups but different backbone lengths. The analysis of the sensing signals are focused on three main FET parameters: (i) changes in the threshold voltage, (ii) changes in the carrier mobility, and (iii) changes in the on-current, compared to the baseline values under vacuum. Using discriminant factor analysis, the performance of the molecularly modified SiNW FETs is further analyzed as sensors array. The combination of sensors having the best discriminative power between the various VOCs are identified and discussed in terms of their constituent surface modifications.

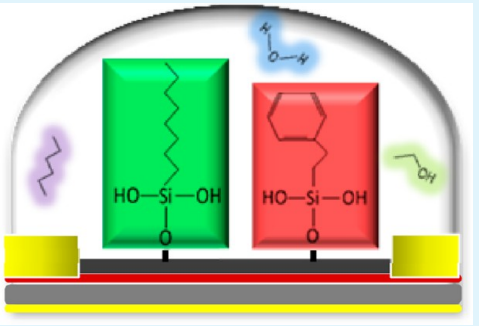

KEYWORDS: *silicon nanowire, field effect transistor, surface modification, volatile organic compound, discriminant factor analysis (DFA)*

INTRODUCTION

The demand for fast, low-cost detection and online monitoring of volatile organic compounds (VOCs) has increased over the years in a variety of fields. For example, in the field of health care applications, the detection and identification of VOCs may lead to the development of novel, noninvasive diagnostic methods for a wide range of diseases, including different types of cancer,[1−10] tuberculosis,[11,12] kidney failure,[13,14] Parkinson's disease,[15,16] and many others (cf. recent reviews and references 2, and 17−20). In this field, VOCs are used as disease biomarkers that are released from the infected area(s) to the bloodstream, from where they are emitted to the exhaled breath, skin, and urine. In the fields of workplace safety and environmental monitoring, there is a growing need for monitoring VOCs from exogamic sources, mostly from industrial processes,[21,22] that could be hazardous, even at very low levels,[21] to humans, animals, and plants.[23]

An emerging approach for the detection of VOCs is based on (semi-) selective recognition by means of silicon nanowire (SiNW) field effect transistors (FETs).[24−29] Sensors based on SiNW FETs have clear advantages over other sensing platforms:

- In comparison with nanomaterial-based chemiresistors,[30−33] SiNW FETs provide additional degree(s) of freedom in operation and/or sensing. More specifically, SiNW FETs allow tailoring the response not only by the voltage applied between the adjacent (source and drain) electrodes, but also by a gate voltage.[27,34] Hence, SiNW FETs allow extracting multiple device parameters that increase the number of independent sensing features per sensor during each measurement.[25−29]
- In comparison to organic FETs, SiNW FETs offer a wider range of carrier mobility.[35,36] Although the carrier mobility of most 'high-performance' organic FETs fall in the range of 1−10 $cm^2/(V\ s)$ (with the exception of single crystal structure, which may achieve higher values[36]), significantly higher carrier mobility values (1000−1350 $cm^2/(V\ s)$)[35,37] have been reported for SiNW FETs. Additionally, the carrier mobility of SiNW FETs can be controlled by a deliberate modification of the constituent synthesis,[38,39] by the number of SiNWs that lie between the source and drain electrodes,[40] and by other factors.
- In comparison to CNT-based sensors, SiNWs are always semiconducting and the semiconducting-metallic transition is less affected by the chirality and the diameter.[41] Furthermore, SiNWs can be more easily integrated into standard VLSI fabrication and processing than CNTs.[42−44]

In addition to these advantages, the ability to tailor the surface chemistry of the SiNW surfaces by layers of (bio) chemical modification[34,45−51] affects the device's stability,[48,52] enhances the electrical properties,[25−29] and widens the possibilities for the interactions between the SiNWs and the VOCs.[1−19,21,23,53] Despite these prominent advantages, the currently available SiNW FETs have drawbacks. The sensing capabilities of SiNW FETs toward nonpolar VOCs are significantly reduced compared to the detection of polar VOCs.

Received: August 15, 2013
Accepted: September 27, 2013
Published: September 27, 2013

Table 1. List of Silane Molecules Used in This Study

group	no. of sensor	name	formula
end group	1	trichloro(3,3,3-trifluoropropyl)silane	$F_3C_3H_4Cl_3Si$
	2	(3-bromopropyl) trichlorosilane	$BrC_3H_6Cl_3Si$
	3	(3-aminopropyl) trimethoxysilane	$NH_2(CH_2)_3(OCH_3)_3Si$
	4	trichloro(phenethyl)silane	$C_8H_9Cl_3Si$
	5	1H,1H,2H,2H-perfluorodecyltrichlorosilane	$F_{17}C_{10}H_4Cl_3Si$
chain length	6	trichloro(hexyl)silane	$C_6H_{13}Cl_3Si$
	7	trichlorododecylsilane	$C_{12}H_{25}Cl_3Si$
	8	hexadecyltrimethoxysilan	$C_{16}H_{33}(OCH_3)_3Si$
	9	trichloro(octadecyl)silane	$C_{18}H_{37}Cl_3Si$

Table 2. Volatile Organic Compounds (VOCs) Used for the Exposure Experiments

VOC	formula	VOC	formula
n-hexane	$CH_3(CH_2)_4CH_3$	1-decanol	$CH_3(CH_2)_9OH$
n-octane	$CH_3(CH_2)_6CH_3$	buthylether	$(CH_3)_3COCH_3$
n-decane	$CH_3(CH_2)_8CH_3$	cyclohexanone	$(CH_2)_5CO$
ethanol	CH_3CH_2OH	1,3,5-trimethylbenzene	$C_6H_3(CH_3)_3$
1-hexanol	$CH_3(CH_2)_5OH$	chlorobenzene	C_6H_5Cl
1-octanol	$CH_3(CH_2)_7OH$	water	H_2O

In previous studies, we have examined the effect of the molecular layer structure on the sensing properties of SiNW FETs.[25−29] This examination included a systematic monitoring of the influence of the cross-linking between adjacent molecules in the molecular layer,[25−27] the influence of the functional (end) group of the molecular layer,[28] and the influence of the chain length of the molecular layer.[29] These studies indicate that polar VOCs are usually detected through the change of dipole moment of the molecular layer attached to the SiNW and/or electrostatic effect of the polar VOCs on the SiNW channel.[28,29] The sensing of nonpolar VOCs has been associated with indirect interactions between the VOC molecules and the modified molecules on the SiNW surface via molecular gating, including: (i) changes in the dielectric properties of the functional organic monolayer; and (ii) changes in the density of charged surface states at the monolayer/SiO_2 interface.[25−27] In the event of sensing nonpolar VOCs associated with indirect interactions, it was found that the longer the chain length of the molecular layer, the higher VOC molecules adsorbed on SiNW surface, and the higher the sensing response.[29] It was also found that an organic layer could detect both polar and nonpolar VOCs, and that the interaction between electron-withdrawing or electron-donating functional groups and VOC molecules may determine the direction of threshold voltage change.[28] In either case, the effect of the functional group on the shift direction of the threshold voltage was found to be more significant compared to the effect of chain length.[28,29] Moreover, it has been proven that

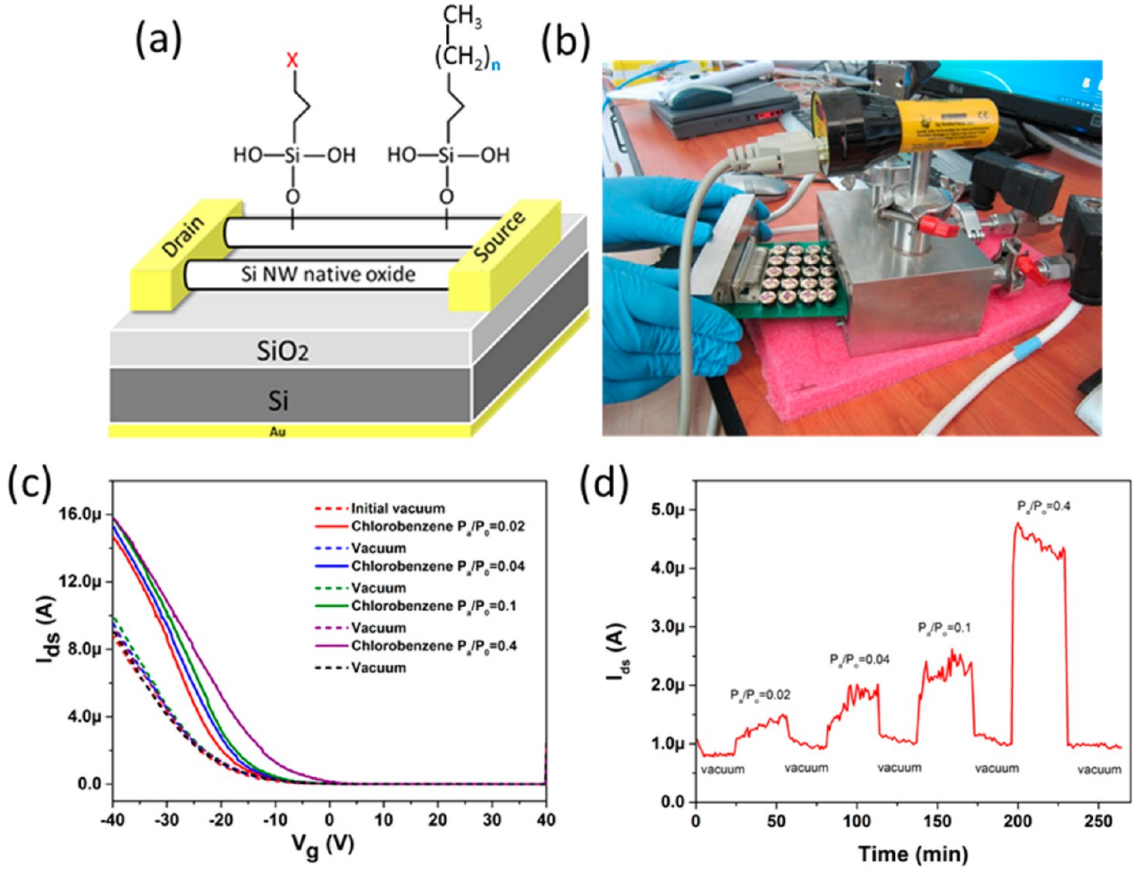

Figure 1. (a) Scheme of SiNW sensor modified with silane monolayers that have either different functional groups or different alkyl chain lengths. (b) Image of the SiNW sensor arrays used in this study. Twenty sensors are loaded on a custom-made circuit board (green color) and VOC exposure measurements are performed in a stainless steel chamber. (c) I_{ds} (at V_{ds} = 2 V) as a function of V_g for sensor S at exposures to chlorobenzene. (**d**) I_{ds} (at V_{ds} = 2 V) as a function of time during an exposure cycle at V_g= −18 V.

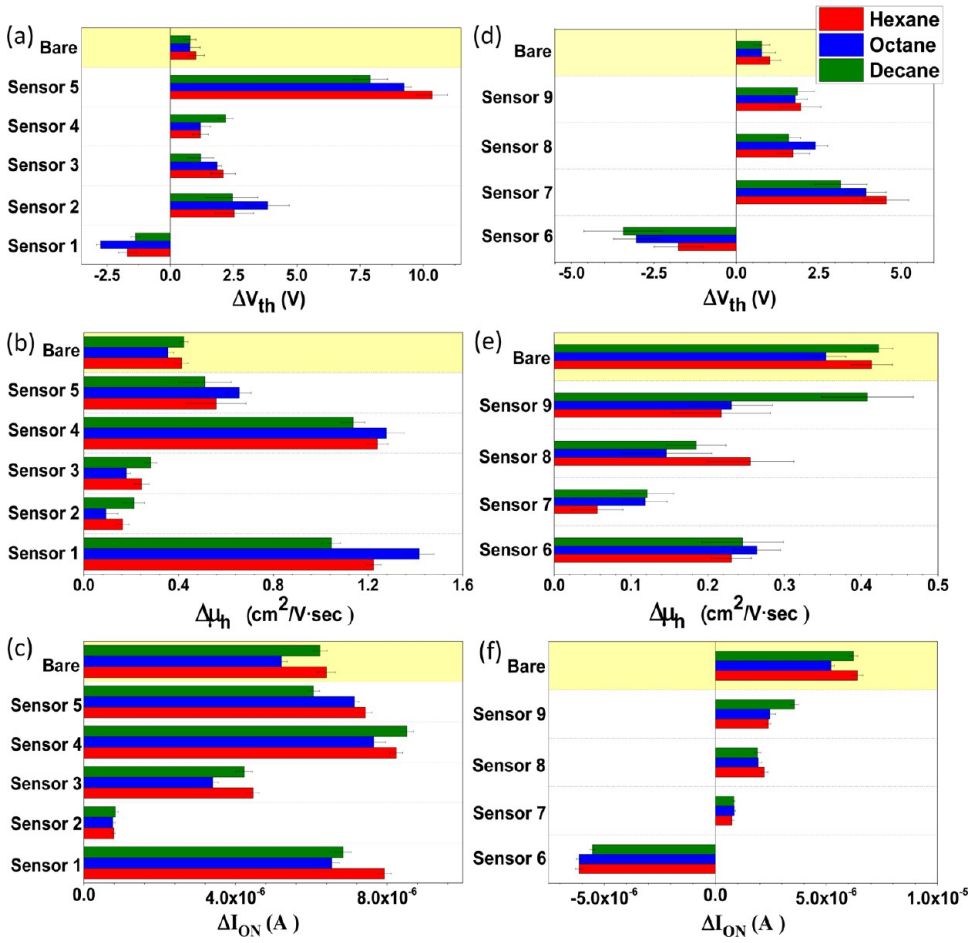

Figure 2. The ΔV_{th}, $\Delta\mu_h$, and ΔI_{ON} of bare and molecularly-modified SiNW FETs upon exposure to nonpolar VOCs at $p_a/p_o = 0.4$. (a–c) Display of the changes in the parameters for different end groups. (d–f) Display of the changes in the parameters for different chain length.

eliminating the trap groups, such as hydroxyl groups (OH), decreases the hysteresis effect and improves the sensing properties even at different levels of humidity.[25]

In the present study, we have explored the sensing performance of SiNW FETs with a variety of surface modifications upon exposure to different polar and nonpolar VOCs in an atmosphere of real-world background humidity (relative humidity: 40%). We have systematically analyzed and compared: (i) SiNW FETs that were functionalized with a series of molecules having different electron-withdrawing and electron-donating end groups; and (ii) SiNW FETs that were functionalized with a series of molecules having similar functional groups but different backbone lengths. The analysis focused on the following sensing parameters of the SiNW FET sensors: (i) changes in the threshold voltage (ΔV_{th}), (ii) changes in the mobility ($\Delta\mu_h$), and (iii) changes in the on-current (ΔI_{on}), compared to the baseline values under vacuum. Furthermore, we have analyzed the discriminative power of sensor-arrays based on different combinations of molecularly modified SiNW FETs, using discriminant factor analysis and leave-one-out cross-validation. The optimized sensor-arrays allowed excellent discrimination between polar and nonpolar VOCs, as well as between the separate VOCs inside each group (polar and nonpolar), even in the presence of a realistic humidity background. The discriminative power of the different sensor-combinations is discussed in terms of their constituent surface modifications.

EXPERIMENTAL SECTION

SiNW Synthesis. p-Type SiNWs having 8.5 ± 1.5 μm length and 40 ± 8 nm diameter were grown on Si substrates by means of chemical vapor deposition, using Au as catalyst and a 1:20 000 gas mixture of SiH_4 and B_2H_6, as described in refs 28 and 54. The grown SiNWs had a single crystalline Si core covered by 5 ± 1 nm of SiO_x and contained pronounced low index facets, such as (111), (100), and (112).[48,55]

SiNW FET Fabrication. The fabrication of FETs based on aligned arrays of Si NWs was described in ref 28. Briefly, the Au catalyst at the opposite end of the grown SiNW attached to the growth substrate, the SiO_x layer coat each Si NW, and the residual Au contamination of the SiNW surface were carefully removed by immersing the SiNWs' growth substrate for 15 s in buffered HF, followed by 2 min of KI:I_2:H_2O (mass ratio 4:1:40). The SiNWs' growth substrate was then placed in a vial with 5 mL ethanol. The vial was introduced into an ultrasonication bath for 6 s to distribute the SiNWs from the growth substrate to the ethanol. The ethanol containing SiNWs was then spray-coated on pre-cleaned SiO_x/Si(100) (p-type; resistivity, 0.001 Ω cm; 300 nm thermal oxide; 10 nm Ti/200 nm Au back gate). The spray coating process (described in ref 55) generated well-aligned NW arrays (~1 NW/100 μm^2).The SiNWs/substrates were then rinsed with acetone, methanol, and ethanol and followed with a treatment of 1 min 50 W oxygen and 5 s buffered HF. Finally, 18 pairs of 10 nm Ti/110 nm Au interdigitated source-drain (S/D) electrodes (length, 1300 μm; width, 2 μm; spacing, 2 μm) were applied on top of the SiNWs by means of photolithography (using Karl Suss MA6Mask Aligner) and lift-off processes, as described in more detail elsewhere.[28] The number of contacted SiNWs with S/D electrodes was examined by optical microscopy (Olympus BX51RF-5; dark field mode) and scanning electron microscopy (e-LiNE, Raith, Dortmund, Germany).

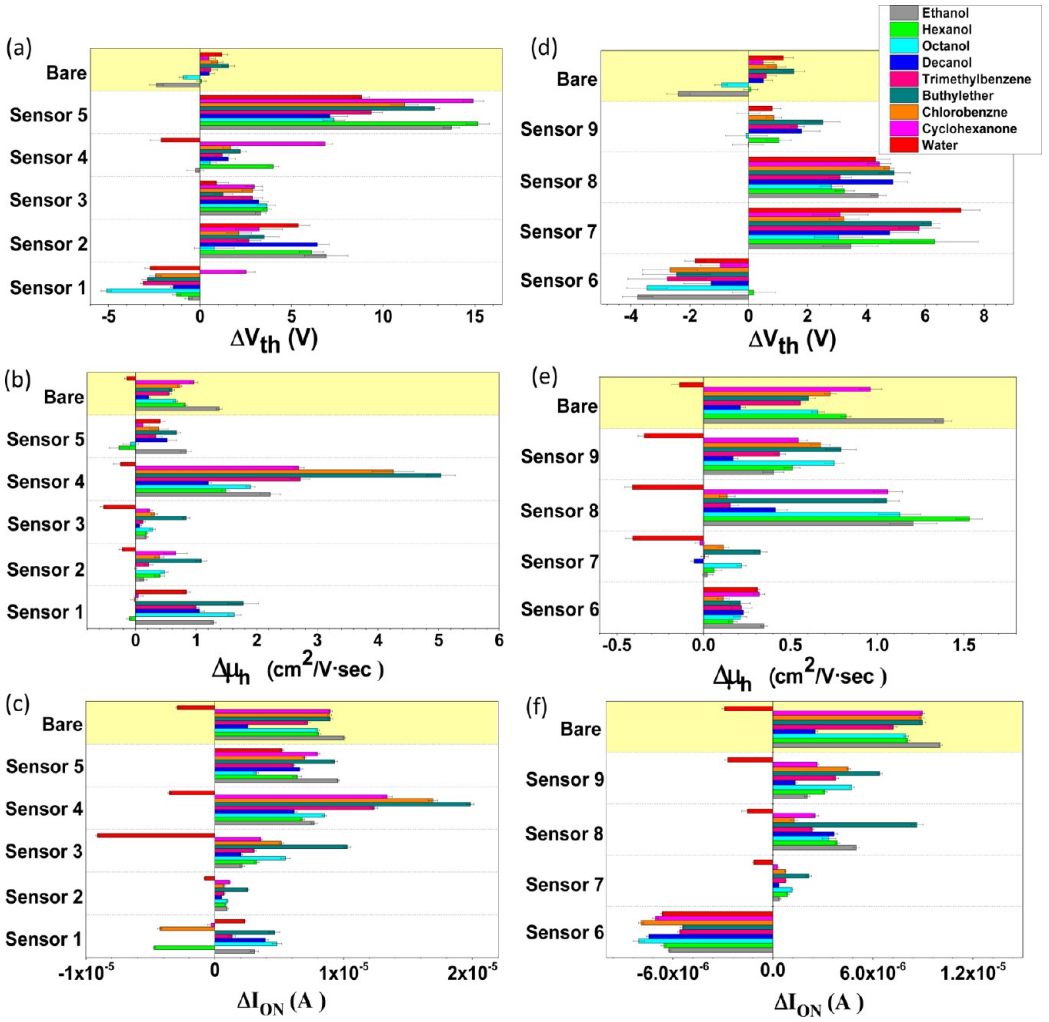

Figure 3. ΔV_{th}, $\Delta \mu_h$, and ΔI_{ON} of bare and molecularly modified SiNW FETs on exposure to polar VOCs at p_a/p_o = 0.4. (a–c) Display of the changes in the parameters for different end groups. (d–f) Display of the changes in the parameters for different chain length.

Modification of the SiNW FETs. The fabricated SiNW FETs underwent a cleaning process which included several steps: (i) sonication in acetone, methanol, and isopropanol for 1 min for each solvent; (ii) drying in spin coater for 1 min at 4000 rpm; (iii) plasma process (30 min, 50 W oxygen). A silane solution was made with toluene solvent for $NH_2(CH_2)_3(OCH_3)_3Si$, $C_8H_9Cl_3Si$, $C_{16}H_{33}(OCH_3)_3Si$ modifications. For the other modifications, the solvent was chloroform. The reaction time for the most of the modifications was 40 min. $C_8H_9Cl_3Si$ and $C_{16}H_{33}(OCH_3)_3Si$ were the exceptional cases, in the sense that the reaction time was 70 min. At the end of the reaction time, all the samples were washed with the same solvent from the preparation solution and were sonicated for 10 min and dried with a spin coater for 1 min at 4000 rpm. The samples were stored in vacuum oven (0.1 mtorr) at 100 °C. Table 1 presents the studied modifications. As seen in the table, the molecular modifications were divided into two main groups: (i) a series of molecules having different electron-withdrawing and electron-donating end groups but with equivalent chain lengths and different linking groups; except for sensor 5, which had a different configuration of the backbone; and (ii) a series of modifications with the same end groups (CH_3) but with different backbone lengths.

Surface Analysis. XPS analysis was performed to verify the presence of the relevant modification on the device's surface. Bare and molecularly modified SiNW arrays on 200 nm Al/Si(100) substrates were tested by X-ray photoelectron spectroscopy (XPS) for surface characterization (Thermo VG Scientific, Sigma Probe, England; monochromatized X-ray Al Kα 1486.6 eV source), as described elsewhere.[28,29] The XPS spectra was analyzed by a peak fitting software (XPSPEAK version 4.1) after subtraction of a Shirley background, while using C 1s (C–C) peak at 285.0 eV as a reference for binding energy calibration. Evaluation of the surface layer thickness was made by spectroscopic ellipsometer (SE, M-2000 V, J. A. Woollam Co., Inc.). Bare and molecularly modified SiO_x/Si substrates were tested at 60, 65, 70, 75, and 80° incidence angles on an open sample stage, as described elsewhere.[28] The molecular layer thickness was determined by a three-phase functional layer/native oxide/Si(111) model. An absorption-free Cauchy dispersion of the refractive index with values of n (1.46 at 1000 nm, 1.61 at 250 nm) was assumed for all molecular cap-layers. Thickness assessment was made by examining the samples before and after modification.

Sensing Measurements of the Modified SiNW FETs. The fabricated SiNW FET devices were bonded to TO-5 holders and loaded to a custom-made circuit board. The circuit board was then inserted into a stainless steel chamber (total volume of ~100 mL) connected to a set of device analyzers. The sensing measurements to VOCs' exposures were performed using Keithley 2636A system SourceMeter and Keithley 3706 system Switch/Multimeter. A Labview-controlled automated flow system delivered pulses of VOCs at controlled concentrations. In a typical experiment, sensors were kept for 15 min in vacuum, followed by 20 min of VOC vapor in air, followed by another 5 min of vacuum environment to purge the system. Electrical measurements of source–drain current (I_{ds}) vs. back gate voltage (V_g) at source–drain voltage (V_{ds}) of 2 V were recorded prior, during, and after the exposure. The VOC vapor was generated

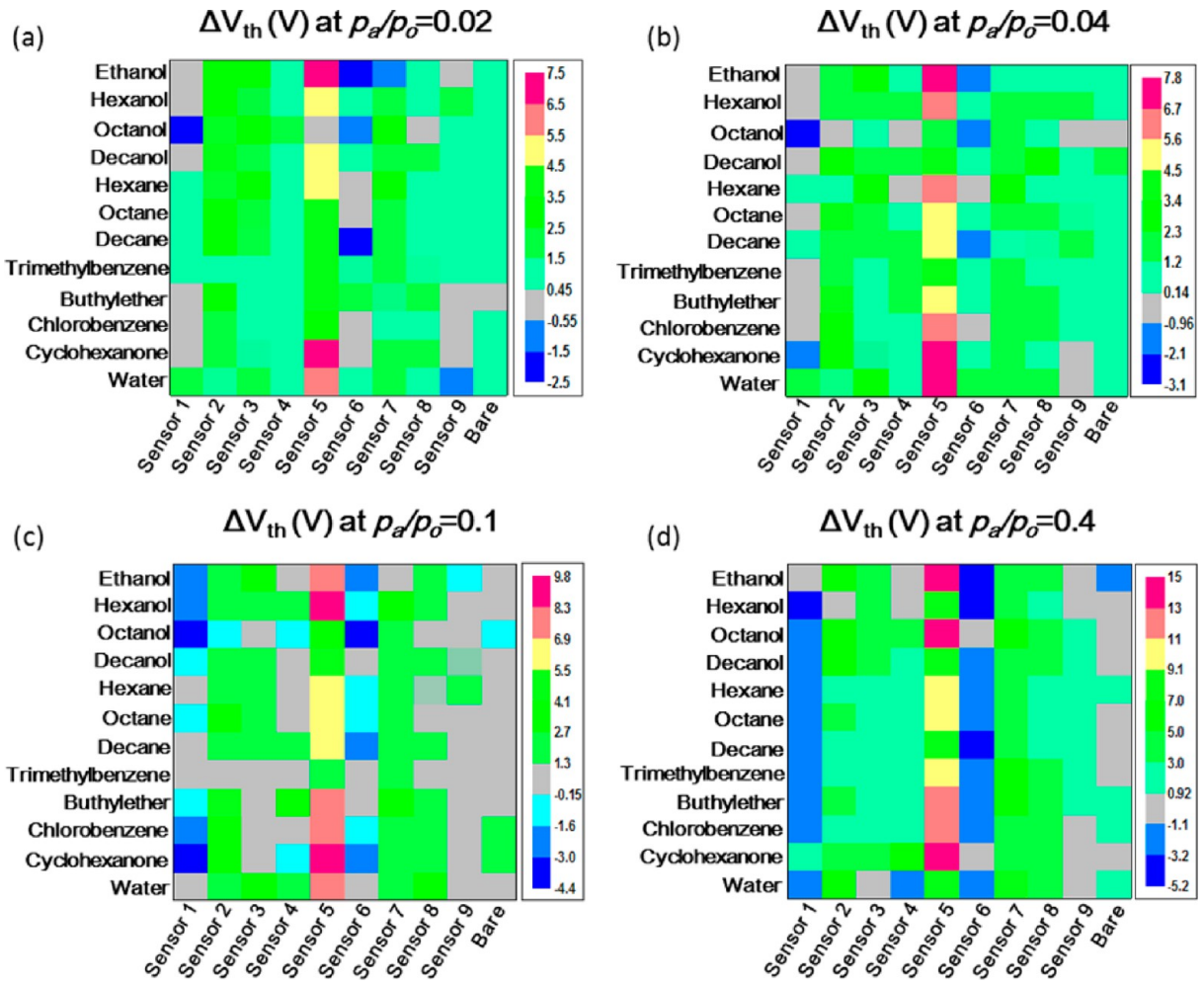

Figure 4. ΔV_{th} (V) for all the studied sensors at various p_a/p_o values: (a) p_a/p_o = 0.02; (b) p_a/p_o = 0.04; (c) p_a/p_o = 0.1; (d) p_a/p_o = 0.4. The values were calculated by subtracting the average value of the initial vacuum step from the average value of the exposure to VOC.

through a bubbler system. Air was bubbled into VOCs liquid phase. As a result, vapors from the VOCs were formed. Four increasing concentrations of vapor in air were tested, p_a/p_o= 0.02, 0.04, 0.1, and 0.4 (p_a and p_o represent VOC's partial pressure and the total vapor pressure, respectively). The measurements were performed at ambient humidity background of 40% relative humidity. The background humidity was introduced as a real-world confounding factor. Table 2 lists the examined VOCs in the experiment.

Data Analysis. The following parameters were extracted for each sensor response: (i) changes in the threshold voltage (ΔV_{th}), (ii) changes in the carrier mobility ($\Delta \mu_h$), and (iii) changes in the on-current (ΔI_{ON}), compared to the baseline values under vacuum. Discriminant Factor Analysis (DFA)[56] was performed for an advanced discrimination between different VOCs. DFA is a supervised, linear method based on a training set of classified information. In this method, new orthogonal axes (canonical variables) are found as a linear combination of the input variables. These factors are calculated to: (i) minimize the variance inside each class, (ii) maximize the variance between the different classes. Leave one out cross-validation method calculates the discrimination accuracy. Given n measurements, the DFA was computed n times using $n - 1$ training vectors. The vector left out during the training part is projected onto the DFA model which was built, creating a discrimination result. The discrimination accuracy is valued as the averaged performance over the n tests.

Statistically significant differences (p-values) between canonical variables of the different classes were studied using the Wilcoxon test, a non-parametric statistical test for data that is not normally distributed. Values $p < 0.05$ were considered to be a significant statistical separation between the two tested classes.

RESULTS

General Electrical Characteristics of the FETs. Two sets of SiNW FETs were prepared as described in the Experimental Section. The first set incorporated a series of molecules with different end groups but with equivalent chain lengths and different linking groups; except for sensor 5, which had a different configuration of the backbone. The second set incorporated a series of modifications with the same end groups (CH_3) but with different backbone lengths and different linking groups. The XPS and ellipsometry results agreed well with the results reported previously[28,29] and confirmed the presence of a monolayer on the surface for all the sensors.

Figure 1a presents a schematic illustration of the molecularly modified SiNW FETs and Figure 1b presents a photo of SiNW FET arrays used in this study. Figure 1c shows the recorded I_{ds} vs. V_g data of sensor 5 at exposures to chlorobenzene as a representative example. As seen in Figure 1c, the I_{ds} values were similar for all vacuum steps. At the same V_g, on exposure to chlorobenzene, the I_{ds} increased compared to the vacuum steps (Figure 1d). The higher was the p_a/p_o of chlorobenzene the higher the I_{ds}. On the basis of the series of measured I_{ds} vs. V_g curves, ΔV_{th}, $\Delta \mu_h$, and ΔI_{ON} (I_{ON} is defined as the I_{ds} at

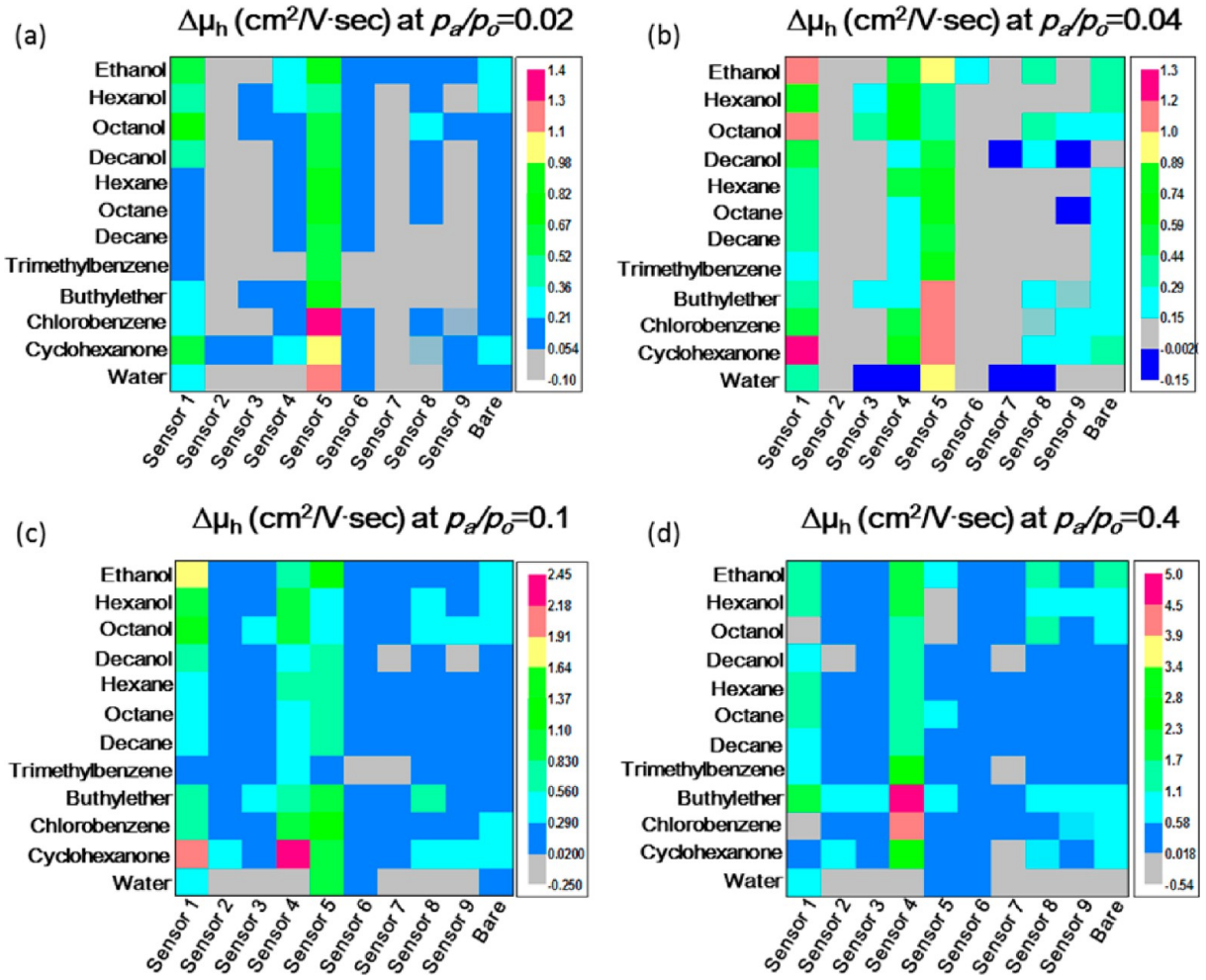

Figure 5. $\Delta\mu_h$ ($cm^2/(V\ s)$) for all the studied sensors at various p_a/p_o values: (a) p_a/p_o =0.02; (b) p_a/p_o = 0.04; (c) p_a/p_o = 0.1; (d) p_a/p_o = 0.4.

V_g = −40 V) were calculated on exposure to VOCs. The results were plotted in Figures 2 and 3.

Effect of the End Group on the Responses to Nonpolar VOCs. As a control, the responses of SiNW FET without molecular layer modification (bare SiNW FET) were tested. The bare SiNW FET showed the largest response in ΔV_{th} on exposure to hexane (Figure 2a). Of all examined modifications, the bare SiNW FET showed the smallest responses in ΔV_{th} on exposure to all tested nonpolar VOCs. Moreover, the bare SiNW FET exhibited the smallest responses in $\Delta\mu_h$ and ΔI_{ON} on exposure to octane amongst all examined VOCs (see Figures 2b and c).

Sensor 1 exhibited negative ΔV_{th} on exposure to all nonpolar VOCs; sensors 2−5 exhibited positive ΔV_{th} on exposure to all nonpolar VOCs (see Figure 2a). Among the tested sensors, sensor 5 displayed the largest ΔV_{th} for all the examined VOCs. The ΔV_{th} of sensors 3 and 5 exhibited a decreasing trend with the increased chain length of the nonpolar VOCs. In contrast, sensors 1 and 2 showed the largest ΔV_{th} on exposure to octane, compared to the other examined VOCs.

All tested sensors exhibited positive $\Delta\mu_h$ values to all nonpolar VOCs (see Figure 2b). For the nonpolar VOCs, sensors 1, 4, and 5 exhibited the largest $\Delta\mu_h$ when exposed to octane, whereas sensors 2 and 3 showed the lowest $\Delta\mu_h$ to octane.

All examined sensors exhibited positive ΔI_{ON} values to all nonpolar VOCs (see Figure 2c). Sensor 2 showed the smallest ΔI_{ON} on exposure to all nonpolar VOCs, compared to other sensors. For nonpolar VOCs, sensors 1, 3, and 4 displayed the smallest ΔI_{ON} on exposure to octane, while sensor 5 displayed a decreasing trend in ΔI_{ON} as the chain length of the nonpolar VOCs increased.

Effect of Chain Length on the Responses to Nonpolar VOCs. Sensor 6 exhibited negative ΔV_{th} values, whereas sensors 7−9 exhibited positive ΔV_{th} values on exposure to all nonpolar VOCs (see Figure 2d). ΔV_{th} of sensor 6 increased with the chain length of the nonpolar VOCs. In contrast, the ΔV_{th} of sensor 7 decreased as the chain length of the VOCs increased. On exposure to octane, the ΔV_{th} of sensors 7−9 decreased as the alkyl chain length of the molecular layers increased.

Sensors 6−9 exhibited positive $\Delta\mu_h$ on exposure to all nonpolar VOCs (see Figure 2e). Moreover, sensors 7 and 9 exhibited increased $\Delta\mu_h$ values as the chain length of the nonpolar VOCs increased. On exposure to octane and decane, the $\Delta\mu_h$ of sensors 7, 8 and 9 showed an increasing trend as the alkyl chain length of the molecular layers increased.

Similar to the trend observed in ΔV_{th}, sensor 6 exhibited negative ΔI_{ON} values, whereas sensors 7−9 exhibited positive values ΔI_{ON} on exposure to all nonpolar VOCs (see Figure 2f). Moreover, the ΔI_{ON} of sensors 7−9 exhibited an increasing trend with increased alkyl chain length of the molecular layers on exposure to all nonpolar VOCs.

Effect of the End Group on the Sensing Signals to Polar VOCs. As shown in Figure 3a, the bare SiNW FET exhibited negative ΔV_{th} on exposure to ethanol and octanol

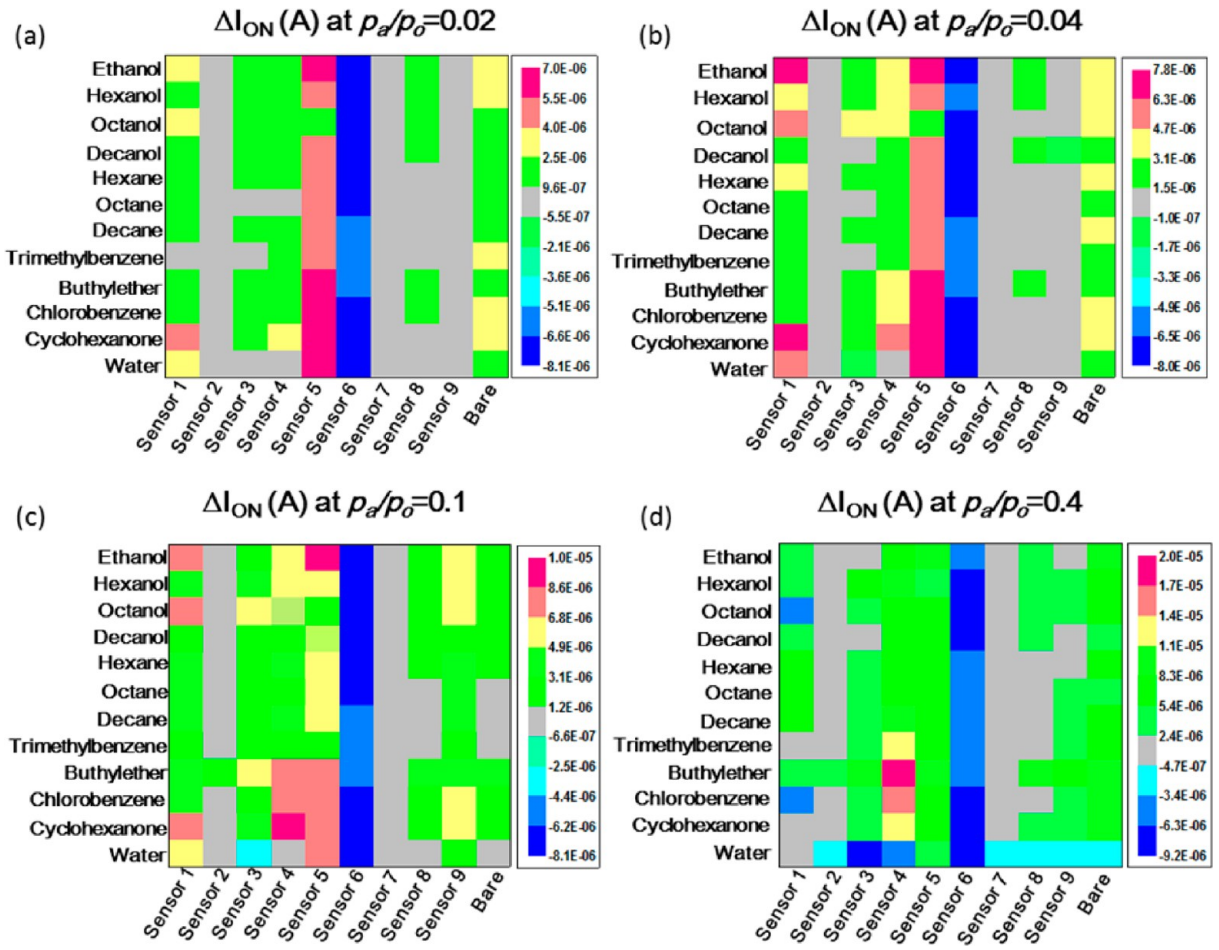

Figure 6. $\Delta I_{ON}(A)$ for all the studied sensors at various p_a/p_o values: (a) p_a/p_o =0.02; (b) p_a/p_o =0.04; (c) p_a/p_o = 0.1; (d) p_a/p_o = 0.4.

Table 3. Classification Accuracy and *p*-Value of the Discrimination between Polar and Nonpolar Groups with Different Sensor Combinations And with a Bare Sensor Alone

	sensor combination	discrimination accuracy (%)	*p*-value
(i)	all sensors	93.75	<0.0001
(ii)	sensors 1−5	66.67	<0.0001
(iii)	sensors 6−9	91.67	<0.0001
(iv)	sensors 3, 4, 5, 6	79.17	<0.0001
	bare	62.50	0.0009

Table 4. Discrimination Accuracy of Groups of Polar VOCs, Nonpolar VOCs and Water with Different Sensor Combinations and with a Bare Sensor Alone

	sensor combination	discrimination accuracy (%)
(i)	all sensors	95.83
(ii)	sensors 1−5	77.08
(iii)	sensors 6−9	85.42
(iv)	sensors 3, 4, 5, 6	75.00
	bare	52.10

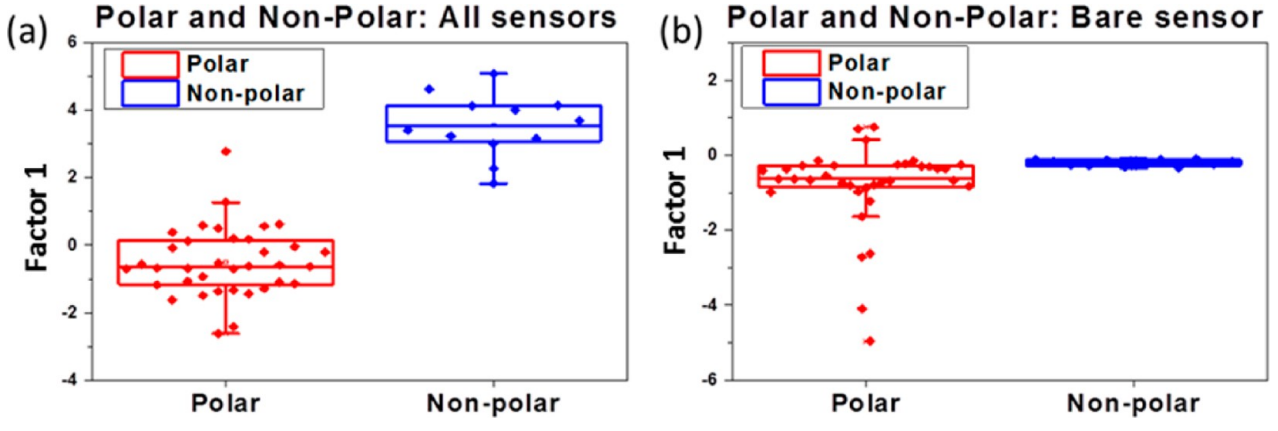

Figure 7. Discrimination accuracy between polar and nonpolar groups by using: (a) A combination of all the studied sensors; and (b) A bare sensor.

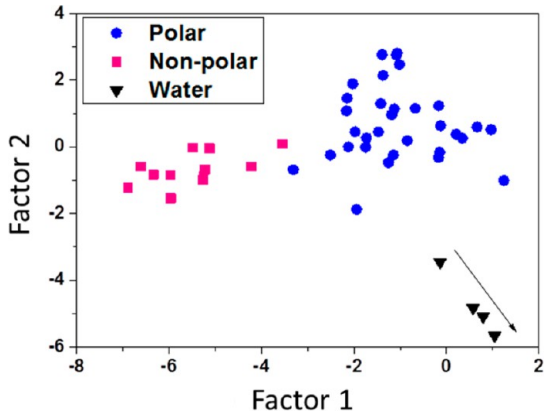

Figure 8. Discrimination accuracy between groups of polar VOCs, nonpolar VOCs and water by a combination of all the sensors. The arrow direction indicates an increasing concentration of water from p_a/p_o = 0.02 to p_a/p_o= 0.4. For the polar and nonpolar groups, this trend was not evidenced.

and nil ΔV_{th} on exposure to hexanol. Exposure of the bare SiNW FET for the rest of the VOCs exhibited positive ΔV_{th}. The largest ΔV_{th} (−2.4 ± 0.39 V) was obtained on exposure of the bare SiNW FET to ethanol.

The bare SiNW FET exhibited negative $\Delta\mu_h$ (−0.14 ± 0.04 $cm^2/(V\ s)$) on exposure to water and positive $\Delta\mu_h$ on exposure to all other examined VOCs (see Figure 3b). The largest $\Delta\mu_h$ (1.38±0.05 $cm^2/(V\ s)$) was observed on exposure to ethanol. The $\Delta\mu_h$ of bare SiNW FET decreased as the chain length of alcohol VOCs increased.

The bare SiNW FET exhibited the largest changes in ΔI_{ON} ($1 \times 10^{-5} \pm 1.03 \times 10^{-7}$ A) on exposure to ethanol and the smallest ΔI_{ON} on exposure to decanol ($2.54 \times 10^{-6} \pm 1.54 \times 10^{-7}$ A). The ΔI_{ON} value for the water exposure was negative ($-2.91 \times 10^{-6} \pm 1.33 \times 10^{-7}$ A). For this sensor, a decreasing trend of ΔI_{ON} was observed as the chain length of alcohol VOCs increased (see Figure 3c).

Sensor 5 exhibited the largest ΔV_{th} for all the VOCs, compared to other sensors (see Figure 3a). Sensors 2, 3, and 5 presented positive ΔV_{th} values for all examined polar VOCs. Sensor 1 displayed positive ΔV_{th} values upon exposure to cyclohexanone, while it showed negative responses to the rest of the polar VOCs. Sensors 1 and 4 were the only sensors that presented a negative ΔV_{th} on exposure to water. Sensor 1 exhibited an increasing trend in ΔV_{th} with the chain length of alcohol VOCs: i.e., ethanol (−0.62 ± 0.2 V), hexanol (−1.29 ± 0.24 V) and octanol (−5.12 ± 0.29 V). In contrast, sensor 2 exhibited a decreasing trend in ΔV_{th} as the chain length of these alcohols increased. A similar decreasing trend in ΔV_{th} as observed in sensor 2 was shown in sensor 5 with the exception of ethanol (i.e. hexanol, octanol and decanol).

Sensors 2−4 exhibited negative $\Delta\mu_h$ for water, while positive for all the other VOCs (see Figure 3b). Among the tested polar VOCs, sensors 1−4 displayed the largest $\Delta\mu_h$ value on exposure to buthylether. As the chain length of alcohol VOCs increased (i.e. ethanol, hexanol and octanol), the $\Delta\mu_h$ of sensor 2 showed an increasing trend. However, no clear chain length dependent trend was observed in the other sensors.

Sensor 2 showed the smallest ΔI_{ON} on exposure to all polar VOCs, compared to sensors 1 and 3−5 (see Figure 3c). Sensor 5 was the only sensor that exhibited positive ΔI_{ON} on exposure to all polar VOCs. Sensors 2−4 presented negative ΔI_{ON} on exposure to water and possible values for all other VOCs. Buthylether presented the largest ΔI_{ON} for sensors 2−4, compared to all other examined polar VOCs. ΔI_{ON} of sensor 3 presented an increasing trend as the chain length of alcohol VOCs increased (i.e. ethanol, hexanol and octanol). Sensor 5 exhibited the largest positive ΔI_{ON} values for ethanol ($9.57 \times 10^{-6} \pm 9.45 \times 10^{-8}$ A) and buthylether ($9.31 \times 10^{-6} \pm 1.85 \times 10^{-7}$ A) and the smallest ΔI_{ON} on exposure to octanol ($3.2 \times 10^{-6} \pm 1.85 \times 10^{-7}$ A) compared to other polar VOCs. As the chain length of alcohol VOCs increased (i.e. ethanol, hexanol and octanol), the ΔI_{ON} of sensor 5 showed a decreasing trend.

Table 5. Discrimination Accuracy of Alcohols, Polar and Nonpolar VOCs, with Individual Sensors and Sensor Combinations at RH = 40%

	discrimination accuracy (%)		
	polar (with water)	alcohols	nonpolar
(i) all sensors	94.44	100.00	83.33
(ii) sensors 1−5	69.44	100.00	83.33
(iii) sensors 6−9	86.11	100.00	83.33
(iv) sensors 3, 4, 5, 6	91.67	100.00	83.33
sensor 1	30.56	56.25	41.67
sensor 2	13.89	50.00	50.00
sensor 3	13.89	62.50	75.00
sensor 4	19.44	37.50	75.00
sensor 5	38.89	93.75	83.33
sensor 6	69.44	100.00	75.00
sensor 7	30.56	62.50	58.33
sensor 8	22.22	37.50	50.00
sensor 9	33.33	62.50	25.00
bare	30.56	50.00	8.33
% of sensors with accuracy above the bare accuracy	30	60	100

Effect of the Chain Length on the Sensing Signals to Polar VOCs. Sensor 9 exhibited the most negligible ΔV_{th} compared to sensors 6−8 (see Figure 3d). Sensor 6 exhibited negative ΔV_{th} for all examined polar VOCs, except for hexanol, which showed a small positive ΔV_{th}. Moreover, sensor 6 displayed the largest ΔV_{th} (−3.76 ± 0.51 V) on exposure to ethanol, compared to the other polar VOCs. Upon exposure to hexanol, trimethylbenzene, buthylether, and water, ΔV_{th} of sensors 7−9 exhibited a decreasing trend as the alkyl chain length of the molecular layers increased. In addition, sensor 7 showed the largest ΔV_{th} (7.22 ± 0.65 V) on exposure to water, compared to all other examined polar VOCs. As the chain length of alcohol VOCs increased (i.e. hexanol, octanol and decanol), the ΔV_{th} of sensor 8 showed a decreasing trend.

Sensors 6 exhibited the positive $\Delta\mu_h$ in response to all polar VOCs (see Figure 3e). On exposure to water, sensor 6 exhibited a positive $\Delta\mu_h$ value, whereas sensors 7−9 exhibited negative $\Delta\mu_h$ value. Sensor 6 displayed the largest $\Delta\mu_h$ (1.38 ± 0.05 $cm^2/(V\ s)$) on exposure to ethanol, compared to the other polar VOCs. Likewise, sensor 9 exhibited the largest $\Delta\mu_h$ (0.79 ± 0.08 $cm^2/(V\ s)$) for buthylether and the smallest $\Delta\mu_h$ on exposure to decanol (0.17 ± 0.03 $cm^2/(V\ s)$). As the chain length of the alcohol VOCs increased (i.e. hexanol, octanol and decanol), the $\Delta\mu_h$ of sensor 8 showed a decreasing trend. Additionally, sensor 8 showed the smallest $\Delta\mu_h$ value for trimethylbenzene and chlorobenzene exposures (0.44−0.67 $cm^2/(V\ s)$) and the largest $\Delta\mu_h$ value for hexanol (1.53 ± 0.08 $cm^2/(V\ s)$). Sensors 7 and 9 exhibited an increasing trend in $\Delta\mu_h$ as the chain length of alcohol VOCs increased (i.e. ethanol, hexanol and octanol).

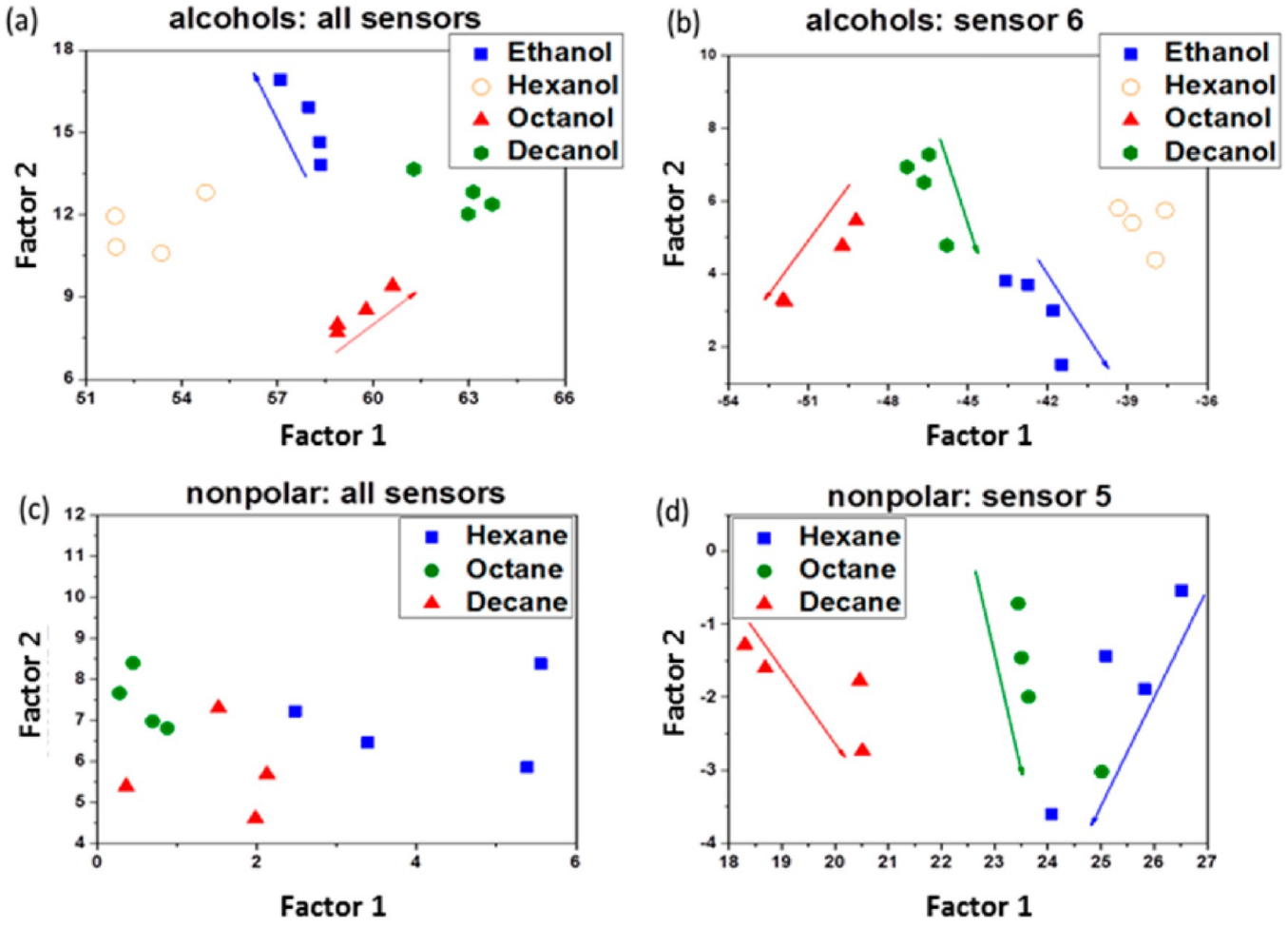

Figure 9. DFA models discriminating the VOCs inside each VOC group: (a) alcohols with a combination of all the sensors; (b) alcohols with sensor 6. The direction of the blue, red and the green arrows indicate a clear trend of increasing concentration (p_a/p_o) of ethanol, octanol and decanol, respectively; (c) nonpolar VOCs with a combination of all the sensors. No clear trend was observed in terms of concentration for each VOC; and (d) nonpolar with sensor 5. The direction of the blue, green, and red arrows indicate a clear trend of increasing concentration (p_a/p_o) of hexane, octane, and decane, respectively.

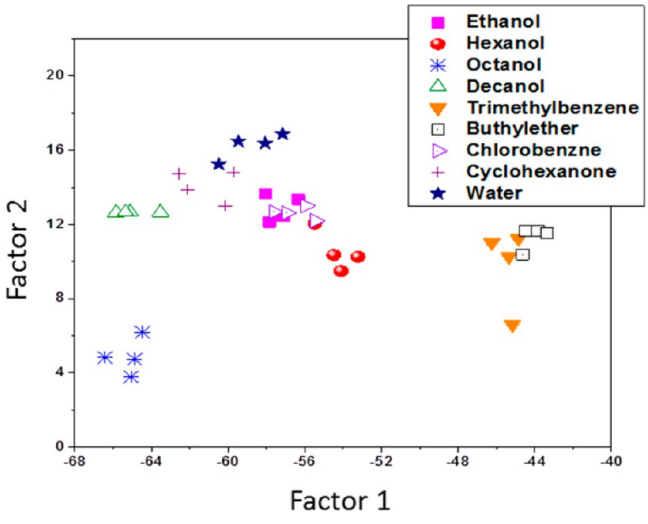

Figure 10. DFA model for discriminating between the VOCs within the polar group with a combination of all the sensors.

Sensor 6 displayed negative ΔI_{ON} values for all examined polar VOCs (see Figure 3f). Sensors 7–9 displayed negative ΔI_{ON} values for water and positive ΔI_{ON} values for the rest of the polar VOCs. Furthermore, on exposure to octanol, trimethylether, chlorobenzene, cyclohexanone and water, the absolute ΔI_{ON} values of sensors 7–9 increased as the alkyl chain length of molecular layers increased. On exposure to alcohols (i.e. ethanol, hexanol and octanol), the ΔI_{ON} of sensors 6, 7, and 9 increased as the chain length of the alcohol VOCs increased. In contrast, the ΔI_{ON} of sensor 8 decreased as the chain length of these alcohol VOCs increased.

DISCUSSION

We have observed a certain variability of the sensing signals V_{th}, μ_h, and I_{ON} for SiNW FETs with different surface modifications. To illustrate this variability, the summarized results from the data analysis which are described in the Results section are presented as hot plots in Figures 4–6. As shown, each sensor responded differently in terms of V_{th}, μ_h, and I_{ON} to the tested VOCs. However, none of the separate sensors showed sufficient chemical and quantitative selectivity to allow precise VOC identification and quantification based on a single sensor alone. Nevertheless, the observed moderate selectivity between the sensors could be exploited for designing flexible, precise and self-learning artificial olfactory systems for specific applications. For this purpose, we have grouped different sensor combinations into

Table 6. Discrimination Accuracy and *p*-Value of Each Polar VOC with Different Sensor Combinations and Individual Sensors

	discrimination accuracy (%) (*p*-value)								
	ethanol	hexanol	octanol	decanol	trimethylbenzene	buthylether	chlorobenzene	cyclohexanone	water
all sensors	100.00	97.22	97.22	94.44	94.44	100.00	94.44	94.44	100.00
	(0.0014)	(0.0014)	(0.0014)	(0.0014)	(0.0014)	(0.0014)	(0.0014)	(0.0014)	(0.0014)
sensors 1−5	88.89	86.11	100.00	94.44	77.78	94.44	94.44	80.56	94.44
	(0.0023)	(0.002)	(0.0014)	(0.0014)	(0.0110)	(0.0020)	(0.0017)	0.0032)	(0.0014)
sensors 6−9	91.67	77.78	97.22	94.44	88.89	100.00	77.78	88.89	86.11
	(0.0014)	(0.002)	(0.0014)	(0.0014)	(0.0014)	(0.0014)	(0.0071)	0.0023)	(0.0014)
sensors 3, 4, 5, 6	94.44	88.89	100	83.33	94.44	91.67	86.11	83.33	97.22
	(0.0014)	(0.0017)	(0.0014)	(0.0023)	(0.0017)	(0.0014)	(0.0017)	(0.0017)	(0.0014)
sensor 1	80.56	55.56	91.67	50.00	58.33	61.11	61.11	69.44	66.67
	(0.0095)	(0.5971)	(0.0017)	(0.1128)	(0.0415)	(0.5627)	(0.0917)	0.0192)	(0.0526)
sensor 2	72.22	63.89	80.56	80.56	63.89	83.33	44.44	69.44	77.78
	(0.0251)	(0.4655)	(0.0038)	(0.0168)	(0.1247)	(0.0220)	(0.4655)	(0.0825)	(0.0045)
sensor 3	61.11	55.56	66.67	63.89	58.33	86.11	50.00	52.78	91.66
	(0.0591)	(0.1993)	(0.0324)	(0.0468)	(0.1019)	(0.0146)	(0.1663)	(0.3201)	(0.0017)
sensor 4	55.56	52.78	63.89	58.33	38.89	72.22	55.56	63.89	91.66
	(0.3263)	(0.4353)	(0.1247)	(0.3263)	(0.8208)	(0.0917)	(0.2368)	(0.1128)	(0.0014)
sensor 5	80.56	69.44	94.44	94.44	63.89	47.22	72.22	66.67	75.00
	(0.0052)	(0.0192)	(0.0027)	(0.0014)	(0.1019)	(0.0739)	(0.0285)	(0.0367)	(0.0061)
sensor 6	75.00	63.89	97.22	77.78%	86.11%	88.89%	80.56%	69.44%	75.00%
	(0.0146)	(0.1247)	(0.0023)	(0.0038)	(0.0110)	(0.0023)	(0.0127)	(0.0367)	(0.0052)
sensor 7	75.00	75.00	55.56	75.00	61.11	77.78	61.11	58.33	80.56
	(0.0110)	(0.0739)	(0.0662)	(0.0082)	(0.1019)	(0.0739)	(0.1376)	(0.1993)	(0.0045)
sensor 8	58.33	69.44	83.33	75.00	47.22	88.89	63.89	66.67	91.66
	(0.0917)	(0.1376)	(0.0027)	(0.0526)	(0.0917)	(0.0220)	(0.1128)	(0.9799)	0.0052)
sensor 9	66.67	77.78	66.67	83.33	80.56	72.22	61.11	72.22	75.00
	(0.0739)	(0.0146)	(0.0739)	(0.0052)	(0.0017)	(0.0367)	(0.0739)	(0.0127)	(0.0038)
bare	80.56	63.89	86.11	75.00	63.89	52.78	75.00	69.44	80.56
	(0.0526)	(0.1376)	(0.0127)	(0.0095)	(0.0662)	(0.5292)	(0.0468)	(0.0285)	(0.0071)
% of sensors with accuracy above the bare accuracy	0	40	30	30	20	80	10	10	30

an array and studied their discriminative power for polar and nonpolar VOCs.

We have evaluated systematically the discriminative power of different combinations of the nine molecularly modified SiNW FETs in this study (see Table 1). For this purpose, we built predictive models for the different sensor arrays, using discriminant function analysis (DFA). The classification success of the DFA models was tested using leave-one-out cross validation.

Discrimination between Polar vs. Nonpolar by SiNW FET Array. We started our systematic comparative study by discriminating between polar and nonpolar groups. We compared the performance of the bare SiNW FET alone to the improved performance of four different sensor combinations: (i) all ten sensors together (nine molecularly modified SiNW FETs and 1 bare Si NW FET); (ii) five SiNW FETs that were functionalized with a series of molecules having different electron-withdrawing and electron-donating end groups; (iii) four Si NW FETs that were functionalized with a series of molecules having similar functional groups but different backbone lengths; and (iv) a selection of four molecularly modified SiNW FETs that contained different end-groups and different chain lengths.

Table 3 lists the *p*-values of the separation in the various DFA models (calculated using Wilxocson test for data that is not normally distributed) and the discrimination accuracy after cross-validation. Foreseeably, combining all ten sensors gave the most accurate results with 94% classification success, whereas the classification by the bare (SiNW FET) sensor was almost random. Clearly, the molecularly modified SiNW FETs showed significantly improved discrimination accuracy between polar and nonpolar groups, compared to the bare sensor. Figure 7 compares the DFA map for these two extreme cases. Combining the sensors that were functionalized with monolayers of different chain length provided a discrimination accuracy of 92%. On the other hand, combining the sensors that were modified with different functional groups produced clearly inferior results in this application (classification accuracy: 67%).

Discrimination between Polar VOCs, Nonpolar VOCs, and Water. In the next step, we have refined the previous application to discriminate polar from nonpolar VOCs other than water. For this purpose we have attempted a three-fold discrimination, treating water vapor samples of different RH levels as separate group of VOCs. The classification accuracies after cross-validation of the different sensor arrays are given in Table 4. The discriminative power was greatly enhanced by including the modified SiNW FETs. As before, the full array of 10 sensors gave the best, near perfect discrimination (see Figure 8), whereas the bare sensor alone produced entirely random results in this case. The discrimination by sensors having different chain length was slightly better than by sensors having different end-groups, but in this application, the differences were less pronounced than for the polarity separation without considering water as a separate group. Indeed, the three sensor combinations (ii), (iii), and (iv) yielded comparable classification accuracy for the present application.

Table 7. Discrimination Accuracy and *p*-Value of Each Nonpolar VOC with Different Sensor Combinations and Individual Sensors

	discrimination accuracy (%) (*p*-value)		
	hexane	octane	decane
All sensors	100.00 (0.0085)	83.33 (0.0085)	100.00 (0.0085)
sensors 1−5	100.00 (0.0085)	83.33 (0.0085)	100.00 (0.0085)
sensors 6−9	75.00 (0.0085)	50.00 (0.1488)	100.00 (0.0085)
sensors 3, 4, 5, 6	91.67 (0.0085)	83.33 (0.0138)	100.00 (0.0085)
sensor 1	58.33 (0.1066)	91.67 (0.0085)	58.33 (0.2696)
sensor 2	58.33 (0.1066)	91.67 (0.0219)	50.00 (0.3502)
sensor 3	91.67 (0.0085)	66.67 (0.0508)	50.00 (0.0745)
sensor 4	66.67 (0.1066)	41.67 (0.2027)	91.67 (0.0138)
sensor 5	83.33 (0.0219)	50.00 (0.5522)	100.00 (0.0085)
sensor 6	83.33 (0.0085)	58.33 (0.4447)	100.00 (0.0085)
sensor 7	75.00 (0.1066)	33.33 (0.9323)	58.33 (0.1488)
sensor 8	66.67 (0.1488)	50.00 (0.4447)	58.33 (0.2696)
sensor 9	16.67 (0.7989)	41.67 (0.3502)	50.00 (0.2027)
bare	16.67 (0.7989)	33.33 (0.2696)	41.67 (0.4447)
% of sensors with accuracy above the bare accuracy	80.00	80.00	100.00

Subclassification of VOCs. Further DFA models were derived to investigate the discrimination accuracy of separate VOCs within well-defined chemical groups (alcohols, other polar and nonpolar compounds) with individual sensors and combinations of the modified sensors. The discrimination accuracy within each group is listed in Table 5. The results for discriminating different polar VOCs from each other varied among the different sensor arrays and showed the same trend that was observed in the previous two applications. However, the discrimination among the alcohols and among the nonpolar VOCs did not vary at all among the different sensor combinations. Perfect classification (100% accuracy) was achieved for the alcohols with all tested combinations, and very good, stable results (83% accuracy) were obtained for the nonpolar VOCs. Interestingly, optimal classification results could be reached for discrimination alcohols (sensor 6) and nonpolar VOCs (sensor 5) with particular single sensors, but not for separating the polar VOCs. Figure 9 compares the DFA models based on all sensors and on the respective single best sensor for the alcohols and nonpolar VOCs. It should be noted that in some of the DFA maps, a clear trend can be seen in terms of the VOC concentration (p_a/p_o). Figure 10 shows the best result (all 10 sensors) for the polar subgroup.

Identification of a Specific Polar VOC by SiNW FETs Array. We have studied the identification of particular polar VOC from among the overall group of the polar VOCs. Table 6 summarizes the discrimination accuracy and the *p*-values for each of the studied VOCs. As could be seen in the table, the combination of all the 10 sensors had the highest discrimination accuracy for all the VOCs. The discrimination accuracy of the sensor array with different chain length was not significantly different from the accuracy of the array having purely end group variations. Some modified sensors showed better discrimination compared to the bare sensor, whereas sensors with other modifications showed inferior results. For the alcohols, chlorobenzene, cyclohexanone, and water, better discrimination accuracy was achieved by the bare sensor (the percentage of the number of the sensors with accuracy above the bare SiNW FET accuracy was under 40%).

Identification of a Specific Nonpolar VOC by SiNW FETs Array. Finally, we have tested the identification of particular nonpolar VOCs from among the group of the nonpolar compounds (see Table 7). We observed that the addition of surface modification significantly improved the ability to discriminate a specific nonpolar VOC from the other nonpolar VOCs. This can also be seen by the discrimination accuracy of each individual sensor and the sensors' combinations compared to the bare sensor.

SUMMARY AND CONCLUSIONS

We have demonstrated that molecularly modified SiNW FETs are powerful tools for VOC detection and discriminations in an atmosphere with real-world background humidity. Three main sensing parameters of the SiNW FETs as compared to the baseline values in initial vacuum were selected as sensing signals: threshold voltage change (ΔV_{th}), mobility change ($\Delta \mu_h$) and I_{on} current change (ΔI_{on}) on exposure to VOCs. A systematic overview was provided of the effect of different types of surface modifications, including different electron-withdrawing, electron-donating end groups, and different backbone lengths. Systematic trends of the surface modification type were established by analyzing the performance of the molecularly modified SiNW FETs as elements of sensor arrays for sensing VOCs. The sensor combinations having optimal discriminative power were identified and discussed in terms of their constituent surface modifications. The optimized sensor arrays allowed excellent VOC discrimination according to their polarity. Additionally, the optimized sensors array allowed excellent discrimination between the separate VOCs inside each group (alcohols, other polar and nonpolar), even in the presence of a realistic humidity background. The results published here show that the sensitivity and accuracy of the cross-reactive array can be tailored to detect the molecules of interest, using appropriate combinations of molecule-terminated Si NW FETs. Ultimately, this approach could lead to the development of cost-effective, lightweight, low-power, noninvasive sensors for the widespread detection of VOCs in real-world applications, including environmental monitoring, homeland security, food safety, and health care devices for disease diagnosis from breath or skin.

AUTHOR INFORMATION

Corresponding Author

*E-mail: hhossam@tx.technion.ac.il.

Notes

The authors declare no competing financial interest.

■ ACKNOWLEDGMENTS

The research leading to these results has received finding from the FP7-Health Program under the LCAOS (Grant 258868). The authors acknowledge Dr. Silke Christiansen (Max-Planck-Institute for the Science of Light, Germany) for providing some of the SiNWs reported in the current study.

■ REFERENCES

(1) Konvalina, G.; Haick, H. *Acc. Chem. Res.* **2013**, DOI: 10.1021/ar400070m.
(2) Broza, Y. Y.; Haick, H. *Nanomedicine* **2013**, *8*, 785−806.
(3) Hakim, M.; Broza, Y. Y.; Barash, O.; Peled, N.; Phillips, M.; Amann, A.; Haick, H. *Chem. Rev.* **2012**, *112*, 5949−5966.
(4) Tisch, U.; Billan, S.; Ilouze, M.; Phillips, M.; Peled, N.; Haick, H. *CML-Lung Cancer* **2012**, *5*, 107−117.
(5) Xu, Z. Q.; Broza, Y. Y.; Ionsecu, R.; Tisch, U.; Ding, L.; Liu, H.; Song, Q.; Pan, Y. Y.; Xiong, F. X.; Gu, K. S. *Br. J. Cancer* **2013**, *108*, 941−950.
(6) Barash, O.; Peled, N.; Hirsch, F. R.; Haick, H. *Small* **2009**, *5*, 2618−2624.
(7) Amal, H.; Ding, L.; B., L. B.; Tisch, U.; Xu, Z. Q.; Shi, D. Y.; Zhao, Y.; Chen, J.; Sun, R. X.; Liu, H.; Ye, S. L.; Tang, Z. Y.; Haick, H. *Int. J. Nanomed.* **2012**, *7*, 4135−4146.
(8) Barash, O.; Peled, N.; Tisch, U.; Bunn, P. A.; Hirsch, F. R.; Haick, H. *Nanomedicine* **2012**, *8*, 580−589.
(9) Hakim, M.; Billan, S.; Tisch, U.; Peng, G.; Dvrokind, I.; Marom, O.; Abdah-Bortnyak, R.; Kuten, A.; Haick, H. *Br. J. Cancer* **2011**, *104*, 1649−1655.
(10) Peng, G.; Hakim, M.; Broza, Y. Y.; Billan, S.; Abdah-Bortnyak, R.; Kuten, A.; Tisch, U.; Haick, H. *Br. J. Cancer* **2010**, *103*, 542−551.
(11) Banday, K. M.; Pasikanti, K. K.; Chan, E. C. Y.; Singla, R.; Rao, K. V. S.; Chauhan, V. S.; Nanda, R. K. *Anal. Chem.* **2011**, *83*, 5526−5534.
(12) Phillips, M.; Cataneo, R. N.; Condos, R.; Ring Erickson, G. A.; Greenberg, J.; La Bombardi, V.; Munawar, M. I.; Tietje, O. *Tuberculosis* **2007**, *87*, 44−52.
(13) Haick, H.; Hakim, M.; Patrascua, M.; Levenberg, C.; Shehada, N.; Nakhoul, F.; Abassi, Z. *ACS Nano* **2009**, *3*, 1258−1266.
(14) Marom, O.; Nakhoul, F.; Tisch, U.; Shiban, A.; Abassi, Z.; Haick, H. *Nanomedicine* **2012**, *7*, 639−650.
(15) Tisch, U.; Aluf, Y.; Ionescu, R.; Nakhleh, M.; Bassal, R.; Axelrod, N.; Robertman, D.; Tessler, Y.; Finberg, J. P. M.; Haick, H. *ACS Chem. Neurosci.* **2012**, *3*, 161−166.
(16) Tisch, U.; Schlesinger, I.; Ionescu, R.; Nassar, M.; Axelrod, N.; Robertman, D.; Tessler, Y.; Azar, F.; Marmur, A.; Aharon-Peretz, J.; Haick, H. *Nanomedicine* **2013**, *8*, 43−56.
(17) Ionescu, R.; Broza, Y.; Shaltieli, H.; Sadeh, D.; Zilberman, Y.; Feng, X.; Glass-Marmor, L.; Lejbkowicz, I.; Mullen, K.; Miller, A.; Haick, H. *ACS Chem. Neurosci.* **2011**, *2*, 687−693.
(18) Tisch, U.; Haick, H. *Rev. Chem. Eng.* **2010**, *26*, 171−179.
(19) Tisch, U.; Haick, H. *MRS Bull.* **2010**, *35*, 797−803.
(20) Konvalina, G.; Haick, H. *ACS Appl. Mater. Interfaces* **2012**, *4*, 317−325.
(21) Wallace, L. A. *Annu. Rev. Energy Environ.* **2001**, *26*, 269−301.
(22) Zilberman, Y.; Ionescu, R.; Feng, X.; Müllen, K.; Haick, H. *ACS Nano* **2011**, *5*, 6743−6753.
(23) Pinto, D. M.; Blande, J. D.; Souza, S. R.; Nerg, A. M.; Holopainen, J. K. *J. Chem. Ecol.* **2010**, *36*, 22−34.
(24) McAlpine, M. C.; Ahmad, H.; Wang, D. W.; Heath, J. R. *Nat. Mater.* **2007**, *6*, 379−384.
(25) Paska, Y.; Haick, H. *ACS Appl. Mater. Interfaces* **2012**, *4*, 2604−2617.
(26) Paska, Y.; Stelzner, T.; Assad, O.; Tisch, U.; Christiansen, S.; Haick, H. *ACS Nano* **2012**, *6*, 335−345.
(27) Paska, Y.; Stelzner, T.; Christiansen, S.; Haick, H. *ACS Nano* **2011**, *5*, 5620−5626.
(28) Wang, B.; Haick, H. *ACS Appl. Mater. Interfaces* **2013**, *5*, 2289−2299.
(29) Wang, B.; Haick, H. *ACS Appl. Mater. Interfaces* **2013**, *5*, 5748−5756.
(30) Ammu, S.; Dua, V.; Agnihotra, S. R.; Surwade, S. P.; Phulgirkar, A.; Patel, S.; K., M. S. *J. Am. Chem. Soc.* **2012**, *134*, 4553−4556.
(31) Kim, I. D.; Rothschild, A.; Lee, B. H.; Kim, D. Y.; Jo, S. M.; Tuller, H. L. *Nano Lett.* **2006**, *6*, 2009−2013.
(32) Salehi-Khojin, A.; Estrada, D.; Lin, K. Y.; Bae, M. H.; Xiong, F.; Pop, E.; Masel, R. I. *Adv. Mater.* **2012**, *24*, 53−57.
(33) Zhang, T.; S., M.; Myung, N. V.; Deshusses, M. A. *Nanotechnology* **2008**, *19*, 332001.
(34) Gao, X. P. A.; Zheng, G. F.; Lieber, C. M. *Nano Lett.* **2010**, *10*, 547−552.
(35) Cui, Y.; Zhong, Z.; Wang, D.; Wang, W. U.; Lieber, C. M. *Nano Lett.* **2003**, *3*, 149−152.
(36) Braga, D.; Horowitz, G. *Adv. Mater.* **2009**, *21*, 1473−1486.
(37) Tang, H.; Zhu, L. G.; Zhao, L.; Zhang, X. J.; Shan, J.; Lee, S. T. *ACS Nano* **2012**, *6*, 7814−7819.
(38) Cui, Y.; Duan, X. F.; Hu, J. T.; Lieber, C. M. *J. Phys. Chem. B* **2000**, *104*, 5213−5216.
(39) Ford, A. C.; Ho, J. C.; Chueh, Y. L.; Tseng, Y. C.; Fan, Z.; Guo, J.; Bokor, J.; Javey, A. *Nano Lett.* **2009**, *9*, 360−365.
(40) Wang, B.; Stelzner, T.; Dirawi, R.; Assad, O.; Shehada, N.; Christiansen, S.; Haick, H. *ACS Appl. Mater. Interfaces* **2012**, *4*, 4251−4258.
(41) Dresselhaus, M. S.; Dresselhaus, G.; Eklund, P. C. *Science of Fullerenes and Carbon Nanotubes*; Academic Press: San Diego, CA, 1996.
(42) Wolf, S., *Silicon Processing for the VLSI Era, Vol. 2: Process Integration*; Lattice Press: Sunset Beach, CA, 1990; p 52.
(43) Wolf, S.; Tauber, R. N., *Silicon Processing for the VLSI Era, Vol. 1: Process Technology*; Lattice Press: Sunset Beach, CA, 2000.
(44) Cui, Y.; Wei, Q.; Park, H.; Lieber, C. M. *Science* **2001**, *293*, 1289−92.
(45) Stern, E.; Vacic, A.; Reed, M. A. *IEEE Trans. Electron Dev.* **2008**, *55*, 3119−3130.
(46) Puniredd, S. R.; Assad, O.; Stelzner, T.; Christiansen, S.; Haick, H. *Langmuir* **2011**, *27*, 4764−4771.
(47) Puniredd, S. R.; Assad, O.; Haick, H. *J. Am. Chem. Soc.* **2008**, *130*, 9184−9185.
(48) Assad, O.; Puniredd, S. R.; Stelzner, T.; Christiansen, S.; Haick, H. *J. Am. Chem. Soc.* **2008**, *130*, 17670−17671.
(49) Bashouti, M. Y.; Stelzner, T.; Berger, A.; Christiansen, S.; Haick, H. *J. Phys. Chem. C* **2008**, *112* (49), 19168−19172.
(50) Bashouti, M. Y.; Stelzner, T.; Christiansen, S.; Haick, H. *J. Phys. Chem. C.* **2009**, *113*, 14823−14828.
(51) Bashouti, M. Y.; Tung, R. T.; Haick, H. *Small* **2009**, *5*, 2761−2769.
(52) Bashouti, M. Y.; Sardashti, K.; Schmitt, S. W.; Pietsch, M.; Ristein, J.; Haick, H.; Christiansen, S. H. *Prog. Surf. Sci.* **2013**, *88*, 39−60.
(53) Engel, Y.; Elnathan, R.; Pevzner, A.; Davidi, G.; Flaxer, E.; Patolsky, F. *Angew. Chem. Int. Ed.* **2010**, *49*, 6830−6835.
(54) Stelzner, T.; Andra, G.; Wendler, E.; Wesch, W.; Scholz, R.; Gosele, U.; Christiansen, S. *Nanotechnology* **2006**, *17*, 2895−2898.
(55) Assad, O.; Leshansky, A. M.; Wang, B.; Stelzner, T.; Christiansen, S.; Haick, H. *ACS Nano* **2012**, *6*, 4702−4712.
(56) Brereton, R. G. *Chemometrics, Application of Mathematics and Statistics to Laboratory Systems*; Ellis Horwood: Chichester, U.K., 1990.